Journal of Inorganic Biochemistry 245 (2023) 112259

Contents lists available at ScienceDirect

Journal of Inorganic Biochemistry

journal homepage: www.elsevier.com/locate/jinorgbio

Evaluation of coumarin-tagged deferoxamine as a Zr(IV)-based PET/fluorescence dual imaging probe

Giammarco Maria Romano [a,1], Virginia Zizi [b,1], Giulia Salvatore [c], Riccardo Bani [c], Monica Mangoni [c], Silvia Nistri [b], Giulia Anichini [c], Yschtar Tecla Simonini Steiner [a], Daniele Bani [b], Antonio Bianchi [a], Andrea Bencini [a], Matteo Savastano [a,*]

[a] Department of Chemistry 'Ugo Schiff', University of Florence, Via della Lastruccia 3, 50019 Sesto Fiorentino, Florence, Italy
[b] Imaging Platform, Department of Experimental and Clinical Medicine, University of Florence, Viale G.Pieraccini 6, 50139 Florence, Italy
[c] Radiotherapy Unit, Department of Experimental and Clinical Biomedical Sciences, University of Florence, Largo Brambilla 3, 50134 Florence, Italy

ARTICLE INFO

Keywords:
Deferoxamine
Zr(IV) - PET imaging
Optical imaging
Dual imaging- metal complexes

ABSTRACT

Desferoxamine (DFO) is currently the golden standard chelator for $^{89}Zr^{4+}$, a promising nuclide for positron emission tomography imaging (PET). The natural siderophore DFO had previously been conjugated with fluorophores to obtain Fe(III) sensing molecules. In this study, a fluorescent coumarin derivative of DFO (DFOC) has been prepared and characterized (potentiometry, UV–Vis spectroscopy) for what concerns its protonation and metal coordination properties towards PET-relevant ions (Cu(II), Zr(IV)), evidencing strong similarity with pristine DFO. Retention of DFOC fluorescence emission upon metal binding has been checked (fluorescence spectrophotometry), as it would – and does – allow for optical (fluorescent) imaging, thus unlocking bimodal (PET/fluorescence) imaging for ^{89}Zr(IV) tracers. Crystal violet and MTT assays on NIH-3 T3 fibroblasts and MDA-MB 231 mammary adenocarcinoma cell lines demonstrated, respectively, no cytotoxicity nor metabolic impairment at usual radiodiagnostic concentrations of ZrDFOC. Clonogenic colony-forming assay performed on X-irradiated MDA-MB 231 cells showed no interference of ZrDFOC with radiosensitivity. Morphological biodistribution (confocal fluorescence, transmission electron microscopy) assays on the same cells suggested internalization of the complex through endocytosis. Overall, these results support fluorophore-tagged DFO as a suitable option to achieve dual imaging (PET/fluorescence) probes based on ^{89}Zr.

1. Introduction

The ^{89}Zr nuclide presents advantageous physical properties (half-life: $t_{1/2}$ = 78.41 h, positron intensity: $I(\beta^+)$ = 22.3%) which made it attractive for positron emission tomography (PET) imaging [1–3]. As for most metal-based drugs and imaging agents, in-vivo release of the oftentimes toxic metal cations must be prevented: a safety feature generally achieved through chelation (for Zr(IV) specifically cf. refs. [1, 4, 5]). Ideally, selected chelator should afford stable, thermodynamically and metabolically, and kinetically inert metal complexes.

As early as 1992 [6], the bacterial siderophore desferoxamine (DFO), a linear chain ligand featuring 3 hydroxamic metal binding moieties, started being investigated as a possible chelator for Zr(IV). The advantages offered by DFO consist first in the suitability of hard hydroxamates for the binding of the hard Zr(IV) ion [7], and in its bifunctional nature (the terminal amino group being easily exploited for antibodies labelling purpose) [5,6,8]. DFO remains to these days the most studied and employed Zr(IV) chelator.

We could argue that easiness of conjugation to antibodies and DFO status of FDA-approved drug (for Fe(III) chelation therapy), rather than long anticipated thermodynamic reasons (hydroxamate were already suggested as ligands for hard ions, Zr(IV) included, by Alfred Werner [9]), were the key to DFO prominence in Zr-based immunoPET [1,4].

The 1965 evaluation of Zr(IV)-benzohydroxamate complex stability

Abbreviations: DFO, Deferoxamine; DFOC, Coumarin tagged DFO as shown in Fig. 1; PET, Positron Emission Tomography; MTT, 3-(4,5-dimethylthiazol-2-yl)-2,5-diphenyltetrazolium bromide; TEM, Transmission Electron Microscopy; FDA, United States Food and Drug Administration; TEA, Triethylamine; ESI MS, ElectroSpray Ionization Mass Spectrometry; DMEM, Dulbecco's Modified Eagle Medium; PBS, Phosphate Buffer Saline.

* Corresponding author.
E-mail address: matteo.savastano@unifi.it (M. Savastano).
[1] These authors equally contributed to this work.

https://doi.org/10.1016/j.jinorgbio.2023.112259
Received 28 March 2023; Received in revised form 9 May 2023; Accepted 16 May 2023
Available online 18 May 2023

by Baroncelli and Grossi [10] (logK_1 (Zr(IV)) = 12.43, logK_1(Fe(III)) = 12.18, extraction method, i.e. < 0.3 log$K$ unit difference for a + 1 increment of cation charge in a hard/hard complex), led to the 1992 first trial [6] under the "zirconium (Zr) forms the most stable metal-hydroxamate complexes known" and "It is expected that this complex is even more stable than the iron-Df (i.e., DFO) complex, which has a log$K$ of 30 (Anderegg et al., 1963 [11])" auspices. Demonstrating such enthusiastic statements proved to be a hard task. Seminal thermodynamic data on simple model hydroxamates appeared only in 2013 [12], defying general basic trends in complex stability [13]. First experimental thermodynamic data for DFO finally appeared in 2018 [14], again generating some debate in binding models and stoichiometry [15], further addressed [16], and hopefully partially solved [17], only lately.

As a matter of fact, the Zr-DFO system presents some metal release issues (some would say "stability", although the term could not be even used in a thermodynamic sense until very recently), with Zr(IV) accumulating in bones [18–20].

Improvement of Zr(IV) chelators remains an active research area to these days, with many candidates of various nature being proposed [1,4,5], among which non-linear, macrocyclic, and even cage-like ones, all of high denticity (hexa-, as DFO, octa-, as suggested by Zr(IV) preference, but also hepta-dentated ligands [21]), and theoretical work being performed in the effort to guide ligand design [22].

In this panorama, DFO still remained of extreme relevance, spawning a well-documented family of bifunctional ligands based on its modification [1,4,5]. Indeed, perfecting an existing system possessing strong advantages could be a suitable way to achieve fitting chelators.

However, the possibilities offered by DFO modification are not limited to enhancing complex stability: as an example, some of us recently prepared a DFO conjugate tagged with a chromophore, which proved useful in probing stoichiometry of Zr(IV)-DFO complexes [17]. Beyond Zr, possibility of obtaining optical response by tagged DFO has been exploited towards its naturally-intended target, Fe(III), in the preparation of a number of fluorescent DFO-based probes intended for Fe(III) monitoring [23,24]. These experience a quenching of fluorescence emission upon the binding of the metal cation. This does not surprise as fluorescence is notoriously inhibited in the presence of paramagnetic species and/or "heavy" elements. Besides the paramagnetic Fe(III) cation, the "heavy" Zr(IV) cation is also expected to inhibit the radiative decay of nearby excited fluorophores.

Conversely, a fluorophore-tagged DFO able to retain its fluorescence even in the presence of Zr(IV) could offer the possibility of pairing PET and optical imaging. This combination would result particularly advantageous, as it couples an expensive, high resolution, non-real time, full-body, and somewhat recent technique (PET), with an inexpensive, real-time, local, long-known one, even though less performing in terms of resolution (optical imaging) [25]. This could be convenient both to assist surgical operations (real time) and to decrease the cost of ex vivo pathology examination, since the expensive PET imaging is nowadays significantly used in drug development.

If the quenching effect invariably observed for Fe(III) would also happen for Zr(IV), then fluorescence-tagged DFO probes would not be suitable for optical imaging, demanding alternative synthetic routes. It must be mentioned here that some fluorescent immunoPET Zr(IV) tracers have been prepared by appending the fluorescent tag elsewhere on the antibody [26]. However, while "heavier" than Fe (Z = 26), Zr(IV) (Z = 40) is a diamagnetic ion. In this sense, we notice that fluorescence quenching effect on a DFO-carbazole conjugate of diamagnetic cations such as Mg(II), Ca(II), and, notably, Zn(II) and Al(III), were found negligible with respect to Fe(III) [24]. Paramagnetic Cu(II) still caused some quenching, yet Mn(II) did not [24].

The chance that Zr(IV) may not reduce fluorescent emission of similar DFO conjugates significantly, providing easy access to fluorescent chelators, is tantalizing in terms of potential imaging applications. To check this working hypothesis the new DFO-Coumarin (DFOC) derivative was prepared (Fig. 1). Among common fluorophores, coumarins present the advantage of being a class of naturally occurring molecules better tolerated than other alternatives (e.g. naphthalene, anthracene, carbazole, etc.…). The DFO structure is such that the hydroxamic portion of the ligand chain, i.e. the metal binding site, is separated by a pentamethylene chain from the functionalized terminal amine. The DFOC conjugate thus present a linker between the binding and signalling units that could be sufficiently long to avoid or reduce the quenching effect associated with the coordination of paramagnetic (Cu (II)) and/or heavy (Zr(IV)) cations.

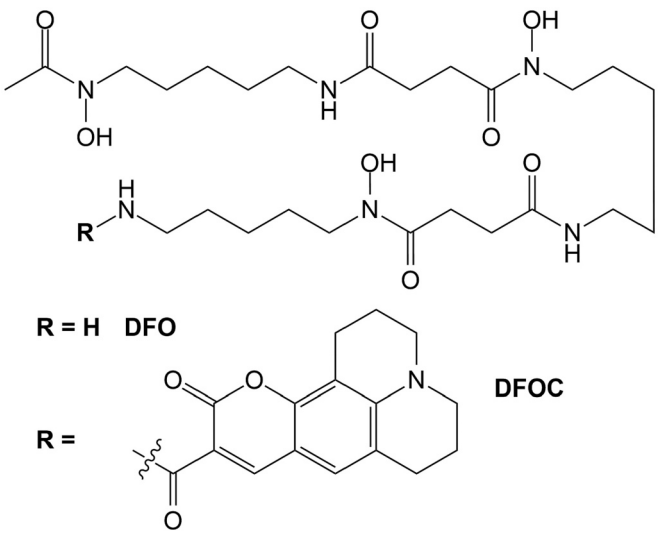

Fig. 1. The DFOC fluorescent conjugate and its parent ligand DFO.

Herein we have analysed the protonation and metal binding properties of the DFOC conjugate (using Cu(II) as test cation), to ascertain the stability of the metal complexes and its absorption/emission properties in the absence and in the presence of metal cations (Cu(II), Zr(IV)), to verify whether the complexes possess the necessary requisite to be used as fluorescent probes in bimodal PET. In view of the possible use of this compound as the basis to develop new photo-radiodiagnostics, we also performed preliminary biological studies on the effects of Zr(IV)-DFOC on normal and neoplastic cell lines in in vitro culture, in order to assess possible dose-related cell toxicity, interferences with cell sensitivity to radiations and biodistribution between the extra- and intracellular compartments.

2. Materials and methods

2.1. Synthesis of DFOC

The synthesis of DFOC (Scheme 1) was adapted from a literature procedure [27,28]. 11-oxo-2,3,5,6,7,11-hexahydro-1H-pyrano[2,3-*f*]pyrido[3,2,1-ij]quinoline-10-carboxylic acid (Coumarin 343 or C343, 1, 199,4 mg, 0.698 mmol) was solubilized in dry CH_2Cl_2 (12 mL) and 15 μL of DMF were added. 2.0 mL of $COCl_2$ were dropped into the solution. The reaction mixture was stirred under N_2 atmosphere for 3 h at room temperature. The solvent was then evaporated under reduced pressure to yield 11-oxo-2,3,5,6,7,11-hexahydro-1H-pyrano[2,3-*f*]pyrido[3,2,1-ij]quinoline-10-carbonyl chloride (2) as a red solid, which was used without further purification. 0.25 mL (1.80 mmol) of TEA were added to a DFO mesylate salt solution (298 mg, 0.453 mmol) in DMF (20 mL) and the solution was stirred under N_2 atmosphere for 10 min. 2 was solubilized in 20 mL of DMF and the solution was slowly dropped into the DFO solution. The reaction mixture was stirred under N_2 atmosphere at room temperature for 16 h. The solvent was evaporated under reduced pressure and then $CHCl_3$ was added. The orange solid was filtered and reprecipitated from DMSO by the addition of some drops of a 1 M HCl

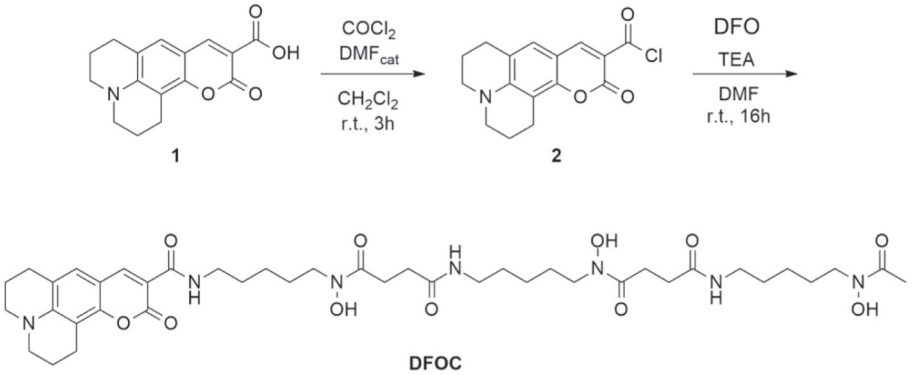

Scheme 1. Synthesis of DFOC.

aqueous solution. (Yield: 213 mg, 57%).

^{1}H NMR (400 MHz, DMSO-d_6): δ(ppm) 9.63–9.59 (m, 3H, H1,2,3), 8.64 (t, 1H, H4, J = 4.00 MHz)), 8.51 (s, 1H, a'), 7.77–7.74 (m, 2H, H5,6), 7.26 (s, 1H, b'), 3.48–3.43 (m, 6H, e, l), 3.36–3.11 (m, 4H, c'), 3.30–3.25 (m, 2H, a), 3.02–2.96 (m,4H, h), 2.76–2.70 (m, 4H, e'), 2.57 (t, 4H, f, J = 8.00 MHz), 2.26 (t, 4H, g, J = 8.00 MHz), 1.96 (s, 3H, m), 1.92–1.84 (m, 4H, d'), 1.55–1.47 (m, 8H, b,d,k), 1.40–1.35 (m, 4H, i), 1.25–1.18 (m, 6H, c,j).). ^{13}C NMR (400 MHz, DMSO-d_6): δ(ppm) 173.04 (C9,9′); 172.37 (C6,6′); 171.20 (C6″); 163.42 (C_p or C_m); 162.99 (C_m or C_p); 153.10 (C_h); 149.01 (C_f or C_n); 148.46 (C_n or C_f); 128.16 (C_i); 120.50 (C_g); 109.14 (C_e); 108.45 (C_l); 105.71 (C_o); 50.61 (C_c or $C_{c'}$); 50.08 ($C_{c'}$ or C_c); 48.17 (C5,5′); 47.87 (C5″); 39.79 (C1); 39.49 (C1',1″); 31.04 (C_a); 29.97 (C2); 29.88 (C2',2″); 28.67 (C8,8′ or C7,7′); 27.88 (C7,7′ or C8,8′); 27.11 (C4,4′,4″); 24.66 (C3); 24.58 (C3',3″); 21.62 (C_d); 21.40 ($C_{b,b'}$); 20.67 (C7″).

Refer to Figs. S1 and S2 for labelling scheme and full spectra.

ESI MS (m/z): 828.9 (z = 1, [DFOC + H]$^+$); cf. Fig. S3 for full spectrum.

2.2. Potentiometric measurements

Potentiometric (pH-metric) titrations, for the determination of the equilibrium constants were performed in 70:30 water:ethanol 0.1 M Me_4NCl at 298.1 ± 0.1 K using an automated apparatus and a procedure that has been previously described [14,17]. The acquisition of the emf data was performed with the computer program PASAT [29,30]. A combined electrode (Metrohm 6.0262.100, Metrohm, Herisau, Switzerland) was calibrated as a hydrogen-ion concentration probe through the titration of standardized HCl solutions with standardized CO_2-free NaOH solutions and by determining the equivalent point using Gran's method [31], which furnishes the standard potential (E°) and the ionic product of water (pKw = 14.06(1) in 70:30 water:ethanol 0.1 M Me_4NCl at 298.1 K). The HYPERQUAD [32] computer program was employed to calculate the stability constants from potentiometric data.

Three measurements were performed to determine ligand protonation constants.

2.3. Spectrophotometric measurements

Absorption spectra were recorded at 298 K on a Jasco V-670 spectrophotometer (Jasco Europe, Lecco, Italy). For the UV–vis spectra, the ligand concentration was 25 μM in all experiments, 25 μM for metals cations (Cu(II) or Zr(IV)) in 1:1 experiments and 50 μM for DFOC:Cu(II) 1:2 titrations. Fluorescence spectra were recorded at 298 K on a FluoroMax Plus spectrofluorometer (HORIBA France, Longjumeau Cedex, France). In all fluorescence experiments the ligand concentration was 1 μM.

2.4. Preparation of Zr:DFOC complex stock solution for bioassay

DFOC (0.62 mg, 7.5 × 10^{-4} mmol) was dissolved in a H_2O/DMSO mixture (5% DMSO, 20 mL). 0.75 mL of a $ZrCl_4$ 10^{-3} M stock solution (in HCl 0.1 M) were added dropwise into the DFOC solution and the pH was adjusted to 5.0. The solution was stirred at room temperature for 1 h. The pH was then adjusted to 6.0 and the mixture H_2O/DMSO (5% DMSO) was added up to a final volume of 30 mL. 20 mL of Zr(IV)-DFOC solution was filtered by using a 0.4 μm RC filter. The final concentration of the solution was spectroscopically determined as 8.0 × 10^{-6} M.

ESI MS (m/z): 914.9 (z = 1, [DFOC + Zr]$^+$); cf. Fig. S4 for full spectrum.

2.5. Citotoxicity assay

The possible toxic effects of the ZrDFOC compound were assayed on normal NIH-3 T3 mouse fibroblasts and neoplastic MDA-MB 231 human mammary adenocarcinoma cells in in vitro culture. In a first experimental set, the effects of this compound on cell viability were assessed on MDA-MB 231 cultures: briefly, the cells were grown in DMEM medium supplemented with 10% foetal bovine serum, 2 mM glutamine, 250 U/mL penicillin G and 250 μg/mL streptomycin, kept at 37 °C in a humidified air atmosphere added with 5% CO_2. ZrDFOC was then added to the culture medium at 0.1, 0.2, 0.4 and 0.8 μM final concentrations for 24 and 48 h. After that, the medium was removed and the cells were stained with crystal violet vital dye (1% in 70% aqueous ethanol, 15 min.), then washed carefully to remove unbound dye, dried and finally dissolved in 10% aqueous acetic acid. The optical density of this violet-colored solution, directly related with the number of viable cells, was measured with a multiplate spectrophotometer (Bio-Rad 550, Milan, Italy) at λ = 595 nm.

In a second experimental set, the effects of ZrDFOC on cell metabolism were assessed on MDA-MB 231 and NIH-3 T3 cultures: briefly, ZrDFOC was added to the culture medium at 0.1, 0.8 and 1.6 μM final concentrations for 24 h. Then, the cells were incubated with MTT, a tetrazolium salt, which is rapidly reduced to insoluble formazan by the cells' mitochondrial enzymes. The formazan crystals were then dissolved in dimethylsulfoxide and the optical density of this purple-colored solution, directly related with cells' oxidative metabolism, read at the spectrophotometer at λ = 540 nm. In both experiments, triplicate experiments were carried out for each cell line.

2.6. Clonogenic survival assay

MDA-MB 231 mammary adenocarcinoma cells were seeded in triplicate into 6-well plates at different densities to achieve singly dispersed cells and incubated in plain culture medium (controls) or medium added with ZrDFOC (0.1 μM). After 1 h, a single dose of 0, 4, 6, or 8 Gy of X-irradiation was delivered by a linear accelerator (Elekta Versa HD©)

Table 1
Cell density at seeding depending on radiation doses.

Cells/well	x-ray dose (Gy)
750	0 (control)
2000	4
2500	6
3000	8

properly set to deliver an exact, homogeneous dose at the level of the cell layers. For each dose, the wells were subdivided in two groups, with or without ZrDFOC, as summarized in Table 1.

After 4 h, the irradiation media were replaced with fresh plain medium and the cells left to grow and checked daily until the survived cells proliferated to give rise to individual colonies, 30–50 cells each. At this time (day 6 post-irradiation), the medium was removed, and the cultures washed in PBS, fixed in buffered formalin and stained with crystal violet. Only separate colonies exhibiting at least 30 cells were counted. The surviving fraction (SF) was calculated by the formula: SF = (mean colony count/seeded cells)x plating efficiency (PE), where PE = mean colony count/cells seeded for unirradiated controls. PE was normalized to the respective control value (ZrDFOC control in combined treatments) for each individual experiment [33]. SF were compared statistically by two-way ANOVA.

2.7. Biodistribution assay

The distribution of the ZrDFOC compound in the extra-and intracellular microenvironments of normal NIH-3 T3 and neoplastic MDA-MB 231 cells were studied by confocal microscopy, exploiting the fluorescent signal of the coumarin moiety. The cells were grown on glass coverslips and ZrDFOC was added to the culture medium at a 0.1 μM final concentration for 10 min., then the coverslip was mounted over a glass slide and observed at a Leica Stellaris 5 (Leica Microsystems, Milan, Italy) confocal microscope equipped with a λ 405 nm excitation laser, setting the spectral sensor at λ 500 nm coincident with the coumarin emission peak, and using a x63 oil immersion objective. Fluorescent and enhanced-contrast (DIC) images were superimposed.

2.8. Transmission electron microscopy

MDA-MB 231 breast adenocarcinoma cells were also studied ultrastructurally to collect additional data on cytotoxicity and cellular uptake of the ZrDFOC compound. This was added to the culture medium at a 0.1 μM final concentration for 10 min., then the cells were detached from the culture plates with a scraper, pelleted by centrifugation at 600*g*, fixed in Karnowsky's fluid, post-fixed in OsO_4 and embedded in epoxy-resin. Ultra-thin sections were cut and observed at a JEM-1010 transmission electron microscope (Jeol, Tokyo, Japan).

3. Results and discussion

3.1. Ligand protonation

As a preliminary analysis for the study of DFOC binding properties, we performed potentiometric measurements coupled with UV–vis absorption titrations to determine the species formed in solution by the ligand and the corresponding protonation constants. DFO conjugation with the fluorophore exploiting its terminal amine (extensively protonated in water, protonation log$K \geq 10.70$), resulted in significant hampering of ligand solubility in water. Therefore, potentiometric titrations where initially performed in mixed solvent (water:ethanol 70:30, 0.1 M NMe_4Cl), where a first protonation constant for the addition of the first two protons ($DFOC^{3-} + 2H^+ = H_2DFOC^-$) and a subsequent protonation ($H_2DFOC^- + H^+ = H_3DFOC$) could be determined. However, sparing solubility of the uncharged H_3DFOC species (below pH 8) and relevance of aqueous media, prompted transport of the study to water (aqueous 0.1 M NMe_4Cl) via UV–Vis absorption spectroscopy instead, which, requiring lower ligand concentration than potentiometry (25 μM vs >0.5 mM), circumvented solubility issues. By UV–Vis, four protonation constants could be determined. Obtained protonation constants are reported in Table 2, while Fig. 2 shows calculated distribution diagram based on spectroscopic constants.

The 4 protonation constants are easily distinguished in two groups: medium to strongly basic, i.e., first three equilibria, corresponding to expected values for the protonation of hydroxamate groups [8], and a

Table 2
Determined equilibrium constants for the protonation of the DFOC ligand in 0.1 M NMe_4Cl at 298 K.

Equilibrium	log $(K)_{pot}$ [a]	log $(K)_{spect}$ [b]
$DFOC^{3-} + H^+ = HDFOC^{2-}$	–	10.57(2)
$HDFOC^{2-} + H^+ = H_2DFOC^-$	–	9.41(5)
$DFOC^{3-} + 2H^+ = H_2DFOC^-$	19.42(2)	19.98(5)
$H_2DFOC^- + H^+ = H_3DFOC$	8.14(8)	8.28(5)
$H_3DFOC + H^+ = H_4DFOC^+$	–	3.11(5)

[a] Potentiometry, 70:30 H_2O:EtOH, 0.1 M NMe_4Cl.
[b] UV–vis spectrophotometry, 0.1 M aqueous NMe_4Cl.

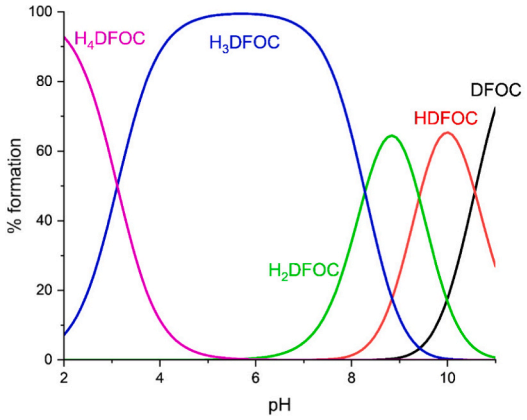

Fig. 2. Species distribution diagram calculated on the basis of spectrophotometric constants. [L] = 25 μM. Charges omitted for simplicity.

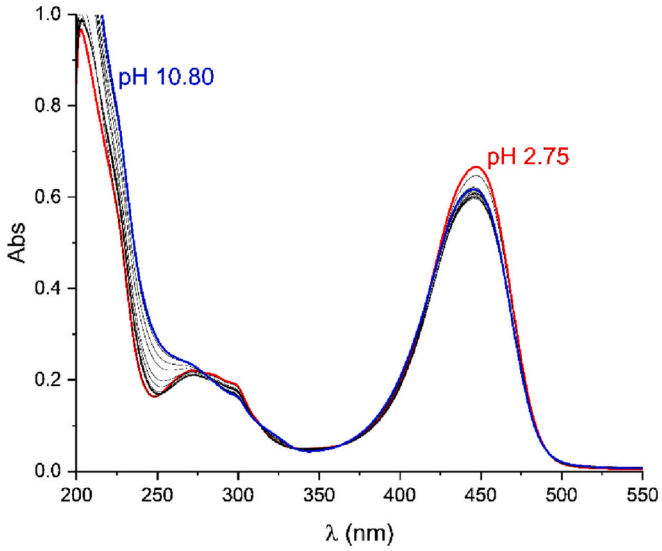

Fig. 3. UV–Vis spectra of DFOC ([DFOC] = 25 μM) in 0.1 M aqueous NMe_4Cl vs pH.

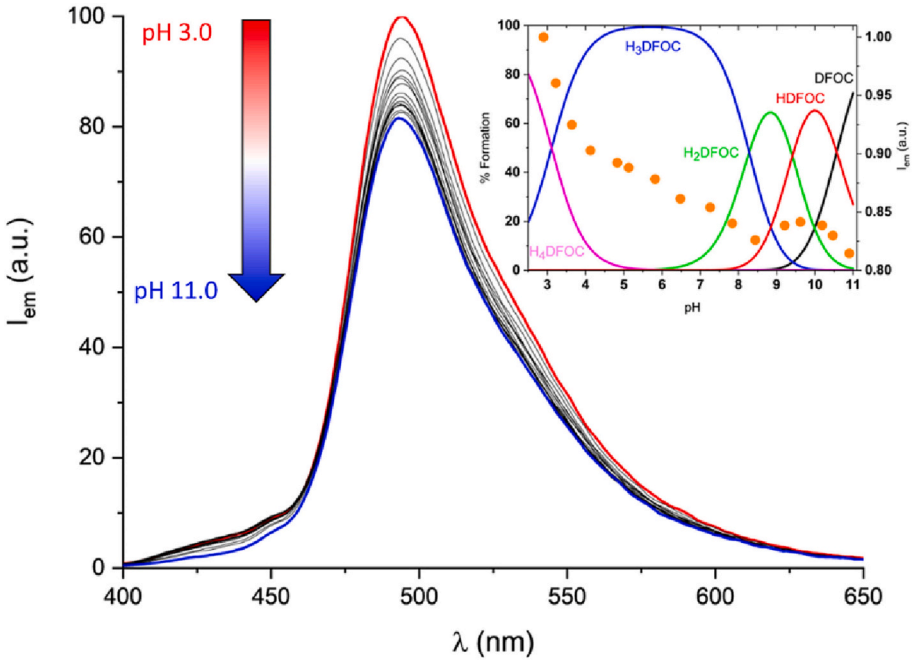

Fig. 4. Emission spectra of DFOC ([DFOC] = 1.0 μM, exc. 390 nm). Inset: variation of fluorescence emission intensity at the 490 nm maximum vs pH.

fourth one, happening in acidic medium. This clearly leads to the predominance of the charge neutral H_3DFOC species at neutral pH. As discussed below, spectral properties suggest that the last equilibrium pertains to the protonation of the tertiary amine introduced with the fluorophore.

UV–Vis absorption spectrum consists of the typical pH dependent band of DFO (below 250 nm) plus bands of the conjugated coumarin (major one centered at 445 nm): these are reported in Fig. 3.

Observed spectral variations are in agreement with proposed protonation pattern as the band pertaining to hydroxamate/hydroxamic acid protonation equilibria (below 250 nm) shows stark variation only for pH > 8 (cf. Figs. 2 and 3). Conversely, coumarin maximum is scarcely sensitive towards hydroxamate protonation, experiencing a significant increase below pH 3.5 instead. Fig. S5 reports overall fit vs wavelength

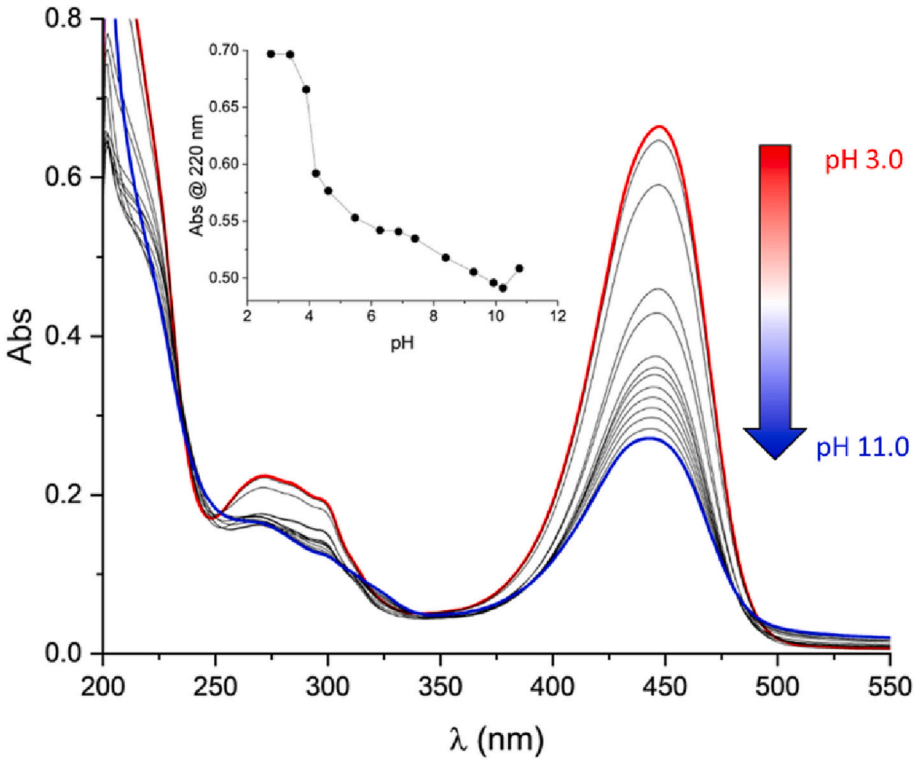

Fig. 5. UV–vis absorption spectrum for the Cu(II):DFOC 1:1 system in 0.1 M aqueous NMe_4Cl ([DFOC] = [Cu(II)] = 25 μM) in the 2.5–11.0 pH range (red to blue). Inset: behaviour of the 220 nm absorption vs pH. (For interpretation of the references to colour in this figure legend, the reader is referred to the web version of this article.)

Table 3
Stability constants of Cu(II) complexes of DFOC determined by UV–vis spectroscopy in aqueous NMe_4Cl 0.1 M. [L] = 25 μM, [Cu(II)] = 25 or 50 μM, two series of spectra in the 2.5–11.0 pH range.

Equilibrium	log *K*
$DFOC^{3-} + Cu^{2+} = [CuDFOC]^{-}$	14.72(4)
$HDFOC^{2-} + Cu^{2+} = [CuHDFOC]$	14.58(3)
$[CuDFOC]^{-} + Cu^{2+} = [Cu_2DFOC]^{+}$	8.73(7)
$[CuHDFOC]^{+} + Cu^{2+} = [Cu_2HDFOC]^{3+}$	4.89(2)
$[Cu_2DFOC]^{+} + OH^{-} = [Cu_2DFOC(OH)]$	4.47(3)

(i.e. experimental vs calculated spectra in the 205–500 nm region) and detail of fits at 220 (hydroxamate) and 445 nm (coumarin) vs pH, showing the behaviour described above.

A similar behaviour was found in fluorescence emission spectra (Fig. 4). The 490 nm emission maximum experiences <20% variation throughout the whole 3–11 pH range, with most of the variation happening in the H_4DFOC^{+} deprotonation to give the H_3DFOC neutral species (i.e., below pH 4).

In brief, it is safe to conclude that, beyond the obvious changes (i.e., conversion of a primary amine to amide group and insertion of a tertiary amine), the functionalization with the fluorophore did not significantly alter the acid/base property of DFO [8], preserving the basic character of the hydroxamate groups.

3.2. Metal binding studies

3.2.1. Cu(II) coordination

Cu(II) was used as a test cation to verify the binding properties of DFOC.

With respect to both Zr(IV) and Fe(III), Cu(II) appears as a more suitable test cation. Not only previous binding studies with plain DFO are plenty [8], but also Cu(II) circumvents both issues related with challenges in determining very high stability constants and those associated with the highly hydrolysable nature, both typical of Fe(III) and Zr (IV). Furthermore, differently from Fe, Cu possesses a positron emitting isotope (^{64}Cu), making it an interesting substrate in itself.

Cu(II) coordination was followed performing UV–Vis spectra of the ligand at different pH values in the presence of 1 or 2 equivs of metals, in order to determine the stoichiometry of the complexes, their formation constants and their distribution in solution as a function of pH. The UV–vis spectra of the Cu(II)-DFOC 1:1 system at various pH are reported in Fig. 5.

Spectra maintain the same main characteristic, although the hydroxamate bands shows stark variations in the acidic instead of the alkaline range (cf. Fig. S5c and Fig. 5 inset): this is due to complexation of the Cu(II) ion which competes with the protons for hydroxamate sites.

Since Cu(II) is known to form also 2:1 M:L complexes with DFO [8], spectra at different pH were recorded also for the 2:1 system (Fig. S6).

The two datasets were then merged and treated simultaneously with the HypSpec [32] software to determine complex formation constants. Obtained values are reported in Table 3 (cf. also Fig. S6 bottom for speciation diagrams).

It is quite natural to attempt at a comparison with Cu(II) complexes stability of the parent ligand DFO.

When the addition of a Cu(II) ion to the fully deprotonated ligand (DFO^{3-}, 3 hydroxamate groups, terminal amino group) is considered, log*K* values range in the 13.54–14.12 range (*I* = 0.1, various ionic media, [8]), while addition of the second Cu(II) ion to the formed CuHDFO complex (3 hydroxamate groups, protonated on the not-coordinating terminal amine) happens with a log*K* in the 7.71–8.30 range (*I* = 0.1, various ionic media, [8]). These values appear in good agreement with those found for Cu(II) complexation by DFOC (addressing species that also have 3 hydroxamate binding sites we have: $DFOC^{3-} + Cu^{2+} = [CuDFOC]^{-}$, log*K* = 14.72, $[CuDFOC]^{-} + Cu^{2+} = [Cu_2L]^{+}$ log*K* = 8.73): this corroborates the idea that conjugation did not affect much the coordination capabilities of the hydroxamate donors.

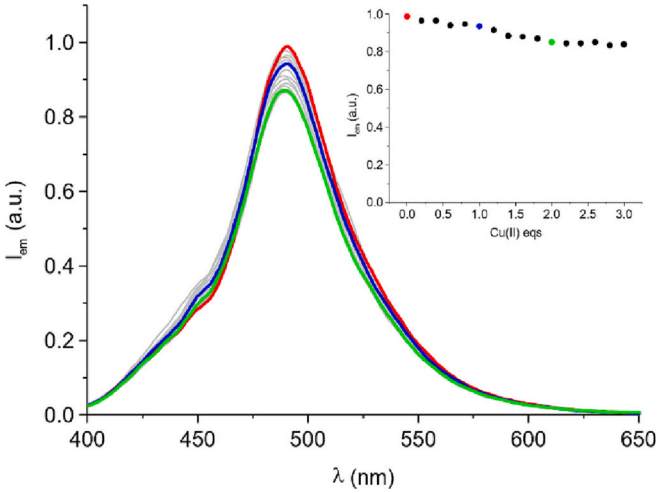

Fig. 6. Fluorescence emission spectra of DFOC ([DFOC] = 1.0 μM, exc. 390 nm) in the presence of increasing Cu(II) equivalents. Inset shows 490 nm emission intensity vs added Cu(II) equivalents.

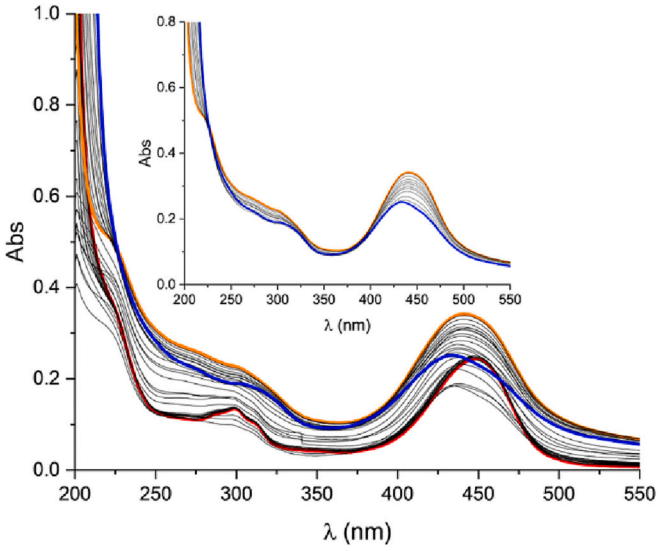

Fig. 7. UV–vis absorption spectrum for the Zr(IV):DOFC 1:1 system in 0.1 M aqueous NMe_4Cl ([DFOC] = [Zr(IV)] = 25 μM) in the 1.9(red)-11.6(blue) pH range. Inset: spectral behaviour in the 9.7(orange)-11.6 (blue) pH range showing a clear isosbestic point at 225 nm. (For interpretation of the references to colour in this figure legend, the reader is referred to the web version of this article.)

As for what fluorescence emission is concerned, Cu(II) coordination is found to have a quite modest quenching effect. Titration of DFOC with increasing equivalents of Cu(II) (0–3 eqs) at pH 8.5 (Fig. 6) show that fluorescent emission of the free ligand is mostly (80% or better) maintained. Such pH was selected as it first leads to the selective formation of the [CuHDFOC] species (0 to 1 added Cu(II) equivalents) and then to $[Cu_2DFOC]^{+}$ one (1 to 2 added Cu(II) equivalents) (cf. Fig. S6 bottom): no remarkable trends due to complex stoichiometry emerge. This result indicates that the length of the spacer separating the metal binding site, e.g. the three-hydroxamate moiety, and the fluorophore is sufficient to inhibit the quenching effect of the Cu(II) paramagnetic ion.

Table 4
Stability constants of Zr(IV) complexes of DFOC determined by UV–vis spectroscopy in aqueous NMe_4Cl 0.1 M.

Equilibrium	log *K*
$DFOC^{3-} + Zr^{4+} = [ZrDFOC]^{+}$	39.3(1)
$HDFOC^{2-} + Zr^{4+} = [ZrHDFOC]^{2+}$	35.9(1)
$H_2DFOC^{-} + Zr^{4+} = [ZrH_2DFOC]^{3+}$	29.4(1)
$[ZrDFOC]^{+} + OH^{-} = [ZrDFOC(OH)]$	2.5(1)

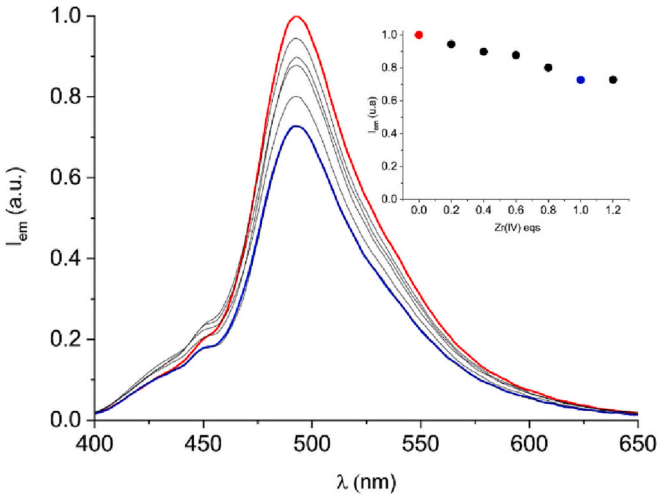

Fig. 8. Fluorescence emission spectra of DFOC ([DFOC] = 1.0 μM, exc. 390 nm) in the presence of increasing Zr(IV) equivalents. Inset shows 490 nm emission intensity vs added Zr(IV) equivalents.

3.2.2. *Zr(IV) coordination*

UV–vis absorption spectra recorded at different pH values were also used to determine the species formed in solution by Zr(IV) and their stability constants. This allow for the evaluation of the pH dependence of the complex stability, a necessary prerequisite for complexes to be exploited as probes for imaging studies of tissues or cells.

Evaluation of Zr(IV) complex stability is notoriously a hard task due to the formation of extremely strong complexes and to the issues brought about by the ion's strong tendency to hydrolyse. According to the 210 nm tail of the hydroxamic acid/hydroxamate band 3 regions can be distinguished (Figs. 7 and S7). First, below pH 3.5, a region possessing a distinguishable trend is found which is furthermore characterized by quick equilibration: this is probably due to the protonation of the coumarin tertiary amine which does not tamper nor involve the metal centre. Then, a noisy region begins, extending up to pH 9.5 characterized by slower equilibration time: perhaps this might depend on non-trivial speciation (e.g. formation of non 1:1 complexes, as reported for DFO [14,16] and DFO-Pym [17]). Then, above pH 9.5, the equilibria return to be fast and the largest spectral variations are observed. Since effect of metalation mimics the one of protonation, the observed spectral variations in alkaline medium are tied to $ZrDFOC^{+} + xOH^{-} = Zr(OH)_x + DFOC^{3-}$ type equilibrium, which sees the hydroxamate groups switching from metalated to deprotonated as Zr(IV) is extracted from the complex due to hydroxide competition (Fig. 7 inset, Fig. S7). Using a previously reported hydrolysis model [14] and assuming only 1:1 complexes are formed (a simplification which is nevertheless true for DFO above pH 9.5, i.e., in the range when hydroxide competition is significant), an estimation of binding constants could be achieved. These are reported in Table 4.

Determined $Zr(IV) + DFOC^{3-} = [ZrDFOC]^{+}$ binding constant is in reasonable agreement with previous values for DFO or its modification [14–17], considering that previous determinations were also done with a different technique (potentiometry) and that binding properties

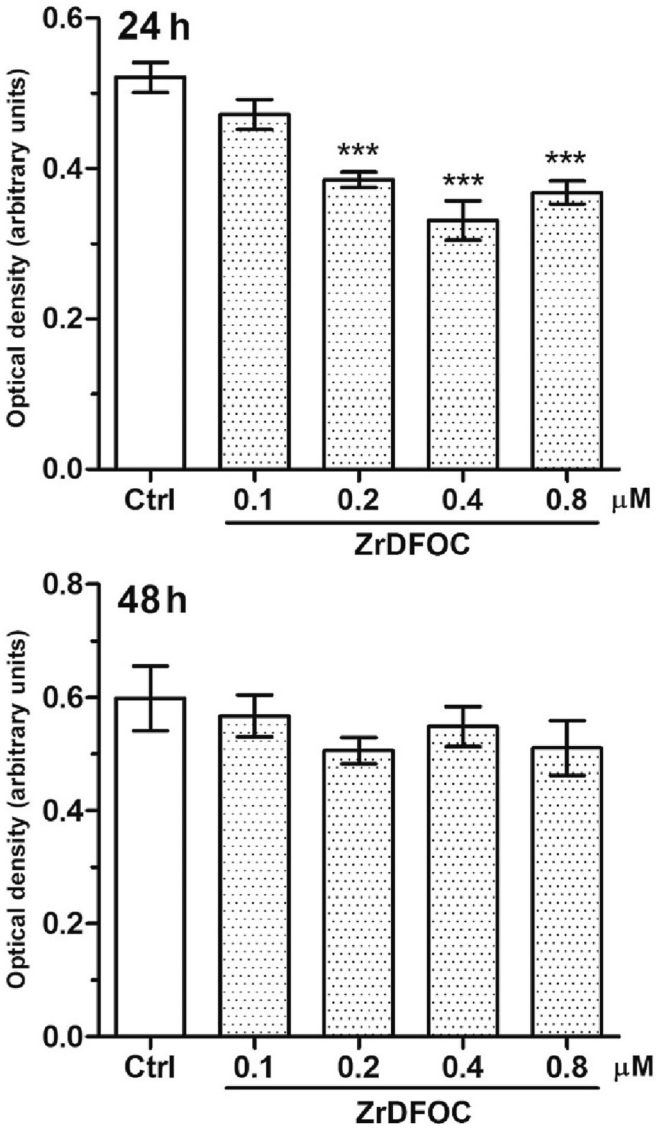

Fig. 9. Cell viability assay by crystal violet vital dye uptake on MDA-MB 231 human breast adenocarcinoma cells exposed to ZrDFOC for 24 and 48 h at the noted concentrations. Only at 24 h was a slight decrease in cell viability detected for concentrations higher than 0.1 μM. Bars are the mean ± SEM of 5 replicate experiments. ***$p < 0.001$ (one-way ANOVA and Newman Keuls post-test). (For interpretation of the references to colour in this figure legend, the reader is referred to the web version of this article.)

evaluation is here done under the 1:1 complexes only a priori assumption. It seems safe to conclude that conjugation with coumarin does not tamper significantly with coordination properties, as suggested also by its protonation properties and complex stability of the Cu(II) test cation.

In terms of emission properties, Zr(IV) is found to tamper little with fluorescence emission (Fig. 8). In fact, by adding increasing amount of Zr (IV) equivalents to DFOC at pH 5.0 (a single species in solution, $[ZrHDFOC]^{2+}$ is formed in solution at this pH under 1:1 complexes assumption), a steady decrease of fluorescence emission is found, although quenching never exceeds a 25%. In terms of stoichiometry of the formed complexes, data clearly indicates that the titration reaches completion after 1 equiv. of Zr(IV) has been added (Fig. 8 inset). Signs of slope change around 0.6 added equivs can perhaps be found, although since fluorescence signal is inherently prone to some noise, the fluorescence emission variation is overall low (the small observed quenching being due to the separation between the fluorophore and the binding group) and working concentration are much lower compared to the case

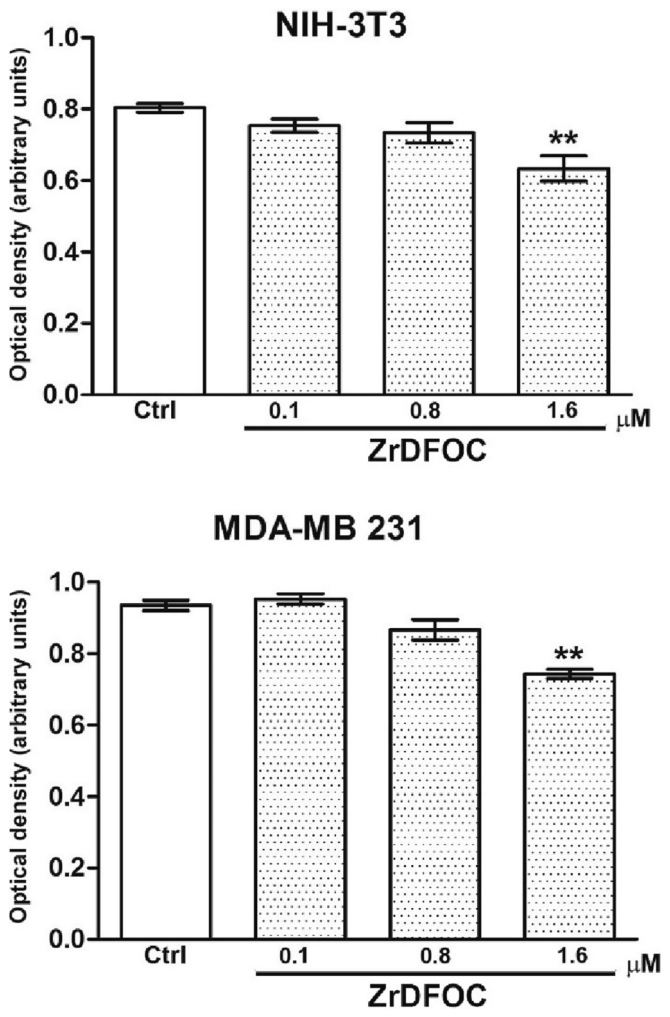

Fig. 10. MTT cell metabolism assay on NIH-3 T3 mouse fibroblasts and MDA-MB 231 human breast adenocarcinoma cells exposed to ZrDFOC for 24 h at the noted concentrations. Only at 1.6 μM was a slight decrease in cell metabolism detected. Bars are the mean ± SEM of 3 replicate experiments. $^{**}p < 0.01$ (one-way ANOVA and Newman Keuls post-test)

where presence of polynuclear complexes could be clearly showed, it is not possible to confidently settle the stoichiometry matter from these data.

In any case, the ZrDFOC complex remains fluorescent and can be optically followed in biological studies: this is exactly the point we intended to prove.

3.3. *In vitro cell tolerability studies*

Two different cell lines, namely NIH-3 T3 normal mouse fibroblasts and MDA-MB 231 human mammary adenocarcinoma cells have been challenged with ZrDFOC to assess its toxicity features.

In a first experimental set, the effects of this compound on cell viability were assessed on neoplastic MDA-MB 231 cell cultures by the crystal violet vital dye assay (Fig. 9). In a second experimental set, the effects of ZrDFOC on cell metabolism were assessed on both neoplastic MDA-MB 231 and normal NIH-3 T3 cell cultures by the mitochondrial respiratory chain MTT assay (Fig. 10). The results of these experiments indicate that ZrDFOC, at the 0.1 μM concentration commonly used in clinical practice for most radiodiagnostics [34], is devoid of cytotoxic effects, as could be argued from its high chemical stability. Indeed, with the crystal violet assay, a slight reduction of the viability of MDA-MB 231 neoplastic cells was only detected at 24 h for concentrations

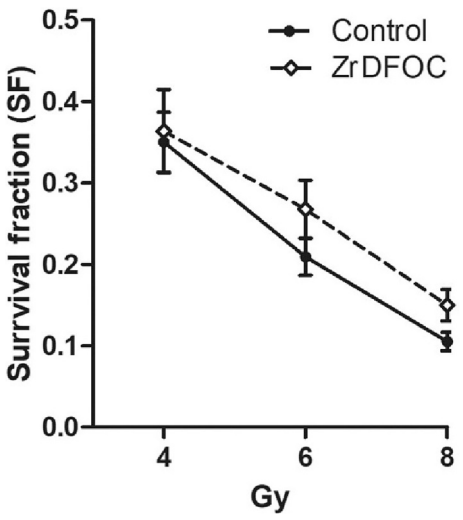

Fig. 11. Survival curves calculated from clonogenic assay of MDA-MB 231 human breast adenocarcinoma cells treated or not with ZrDFOC (0.1 μM) and exposed to X-irradiation at increasing doses. Two-way ANOVA: $P = 0.62$, not significant.

higher than 0.1 μM. This effect was no more detectable at 48 h, conceivably because of the selection of cell clones expressing the multi-drug resistant (MDR) phenotype, characterized by the appearance of plasma membrane efflux pumps for exogenous chemicals [35,36]. In keeping with the above findings, the MTT cell metabolism assay on normal NIH-3 T3 fibroblasts and neoplastic MDA-MB 231 cells exposed to ZrDFOC for 24 h at increasing concentrations showed no significant interference of the compound: only at a >10-fold higher dose was a slight decrease in cell metabolism detected.

3.4. *In vitro radiosensitivity studies*

In view of a possible use of ZrDFOC for the development of new photo-radiodiagnostics, it was important to assess whether this compound would interfere with the sensitivity of neoplastic cells to x-radiation therapy. Ionizing radiations induce cytotoxicity by both direct effects mediated by DNA strand breaks and indirect effects mediated by reactive oxygen species (ROS) in oxygen-containing tissues and evenly targeting nucleic acids, proteins and membrane lipids [37]. In this context, metal chelates have been shown to behave as ROS scavengers, since the metal ion centre can bind the unpaired electrons of ROS radicals catalysing their transformation in inert chemical species [38]. On the other hand, it is known that several molecules can act as radiosensitizers by potentiating the cellular mechanisms of susceptibility to radiations and, in some cases, are used therapeutically as such to reduce the radiation dose [39].

In the present experiment, a clonogenic (i.e. colony-forming) assay was used to evaluate and compare the radiosensitivity of MDA-MB 231 mammary adenocarcinoma cells in the absence or presence of ZrDFOC, following a protocol previously used for similar purposes [33].

As shown in Fig. 11, no significant differences were detected between the two experimental conditions, indicating that ZrDFOC did not interfere, either positively or negatively, with the cytotoxic response of MDA-MB 231 mammary adenocarcinoma cells to increasing X-ray doses (4–8 Gy), like those delivered by linear accelerators for radiotherapeutic purposes.

3.5. *In vitro biodistribution studies*

The same cell lines used for the toxicity studies, NIH-3 T3 fibroblasts and MDA-MB 231 mammary adenocarcinoma cells, were incubated in culture medium added with ZrDFOC (0.1 μM) for 10 min. to investigate

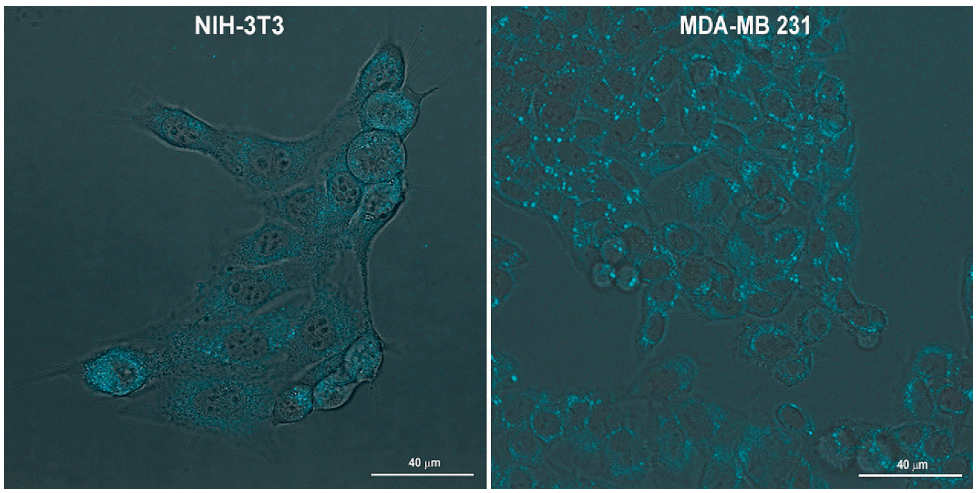

Fig. 12. Merged enhanced-contrast (DIC) and fluorescent (λ 540 nm emission) images of NIH-3 T3 mouse fibroblasts and MDA-MB 231 human breast adenocarcinoma cells exposed to 0.08 µM ZrDFOC for 10 min. A dotted cyan fluorescence can be seen within both cell types, especially in the neoplastic ones. A faint, diffuse cyan fluorescence can also be seen in the background. Confocal microscopy, magnification x630. (For interpretation of the references to colour in this figure legend, the reader is referred to the web version of this article.)

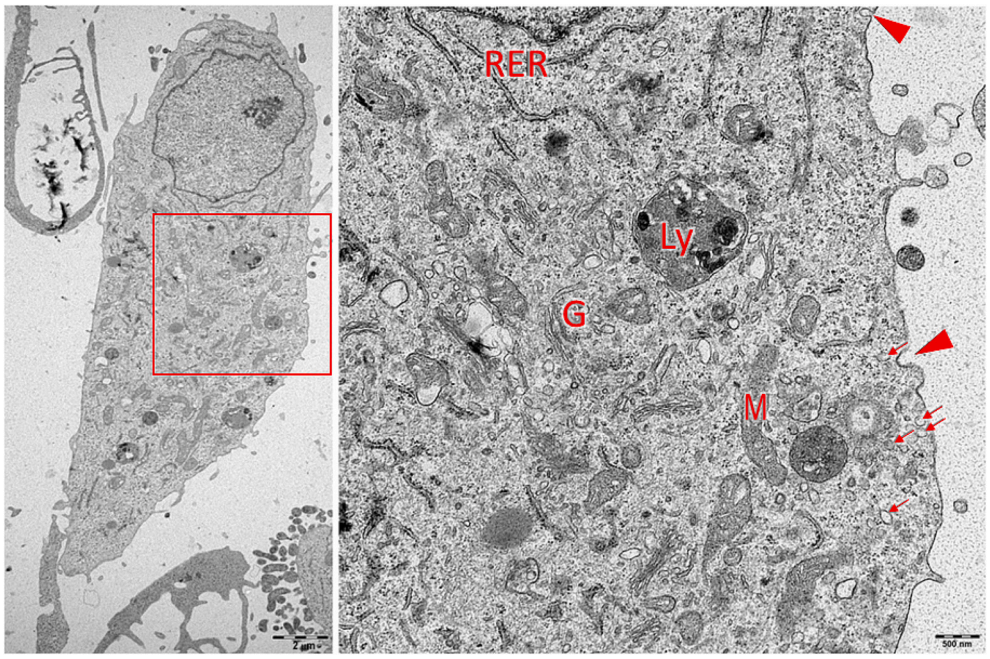

Fig. 13. Representative ultrastructural images of a MDA-MB 231 human breast adenocarcinoma cells exposed to 0.1 µM ZrDFOC for 10 min. This cell shows normal organelles with no signs of damage, some of which are labelled as follows: RER, rough endoplasmic reticulum; G, Golgi apparatus; M, mitochondrion; Ly, lysosome. Plasma membrane pits (arrowheads) and microvesicles in the peripheral cytoplasm (arrows) are suggestive of pinocytosis. Magnification is indicated under the bars.

the extra- and intracellular distribution of this compound, exploiting the λ = 405–540 nm excitation-emission pair of its coumarin moiety as tracking signal (cyan) under a Leica Stellaris 5 confocal microscope. The obtained findings showed a faint, diffuse cyan fluorescence in the extracellular milieu and a more intense, dotted fluorescent signal within the peripheral cytoplasms, suggesting that endocytosis of the compound had occurred (Fig. 12). Of note, this phenomenon appeared more prominent in the neoplastic than in the normal cells, likely because of a higher metabolic activity in the former ones.

To strenghten the results of the above experiment, MDA-MB 231 human breast adenocarcinoma cells exposed to 0.1 µM ZrDFOC for 10 min. were examined under a Jeol JEM-1010 transmission electron microscope. These cells showed a well-developed organellular complement with normal features and no signs of damage. Plasma membrane pits and peripheral microvesicles, suggesting the occurrence of pinocytosis phenomena, were often observed (Fig. 13).

Taken together, the above findings suggest that ZrDFOC per se has a moderate tendency to be uptaken by the cells, likely through the pinocytosis pathway. In perspective, this behaviour could be enhanced and made more selective towards specific target cell types, such as neoplastic cells, by addition of targeting vectors, such as folate or tumor-specific mAbs [40,41] exploiting the ease of functionalization of the DFOC scaffold.

4. Conclusions

Results herein discussed show that coumarin-tagged DFO retains protonation and coordination properties of hydroxamic acids group typical of the parent DFO ligand. Moreover, while fluorescence emission is quenched to some extent by paramagnetic Cu(II) and diamagnetic second row transition metal Zr(IV), the hampering of emissive properties is very modest, never exceeding 20% for Cu(II) and 25% for Zr(IV). This demonstrates how fluorophore-tagged DFO can provide access to dual imaging PET/fluorescence probes based on ^{89}Zr. Moreover, the

ZrDFOC complex appears well tolerated on a cellular level, with no appreciable cytotoxic effect at radiodiagnostic concentrations (0.1 μM). Biodistribution assay suggest endocytosis as internalization mechanism, which can be followed by fluorescent microscopy.

These promising results prompts to further investigation and additional synthetic modification of fluorescent DFO derivatives, tackling especially three aspects. First, it would be important to restore the bifunctional nature of DFO, i.e. a terminal group not involved in Zr(IV) coordination which can be easily conjugated to biomolecules (ideally again a primary amine, so that DFO bioconjugation protocols would tentatively still hold). Second, fluorophore selection could be improved to better cope with the needs of cellular and tissue imaging, i.e., derivatives with longer emission and excitation wavelengths could be devised. Third, selectivity towards tumor cells could be improved by the addition of appropriate targeting vectors to the DFOC scaffold.

With these caveats, we might expect to produce effective dual imaging probes based on ^{89}Zr complexes of fluorophore tagged DFO.

CRediT authorship contribution statement

Giammarco Maria Romano: Investigation, Formal analysis. **Virginia Zizi:** Investigation, Formal analysis. **Giulia Salvatore:** Methodology, Formal analysis. **Riccardo Bani:** Investigation, Formal analysis. **Monica Mangoni:** Methodology, Supervision, Writing – original draft. **Silvia Nistri:** Investigation, Formal analysis. **Giulia Anichini:** Methodology, Formal analysis. **Yschtar Tecla Simonini Steiner:** Investigation, Formal analysis. **Daniele Bani:** Methodology, Supervision, Formal analysis, Writing – original draft, Writing – review & editing. **Antonio Bianchi:** Conceptualization, Supervision, Writing – review & editing. **Andrea Bencini:** Conceptualization, Supervision, Writing – review & editing. **Matteo Savastano:** Investigation, Conceptualization, Writing – original draft, Writing – review & editing.

Declaration of Competing Interest

The authors declare that they have no known competing financial interests or personal relationships that could have appeared to influence the work reported in this paper.

Data availability

No data was used for the research described in the article.

Acknowledgements

Financial support from Italian Ministero dell'Istruzione, Università e Ricerca within the PRIN project 2017EKCS3 is gratefully acknowledged.

We gratefully acknowledge CISM (Mass Spectrometry Centre, University of Florence) for recording ESI mass spectra.

Appendix A. Supplementary data

Supplementary data to this article can be found online at https://doi.org/10.1016/j.jinorgbio.2023.112259.

References

[1] J.R. Dilworth, S.I. Pascu, The chemistry of PET imaging with Zirconium-89, Chem. Soc. Rev. 47 (2018) 2554–2571, https://doi.org/10.1039/C7CS00014F.
[2] M.A. Deri, B.M. Zeglis, L.C. Francesconi, J.S. Lewis, PET imaging with 89Zr: from radiochemistry to the clinic, Nucl. Med. Biol. 40 (2013) 3–14, https://doi.org/10.1016/j.nucmedbio.2012.08.004.
[3] J.P. Holland, M.J. Williamson, J.S. Lewis, Unconventional nuclides for radiopharmaceuticals, Mol. Imaging 9 (2010), https://doi.org/10.2310/7290.2010.00008, 7290.2010.00008.
[4] N.B. Bhatt, D.N. Pandya, T.J. Wadas, Recent advances in Zirconium-89 Chelator development, Molecules 23 (2018) 638, https://doi.org/10.3390/molecules23030638.
[5] I.V.J. Feiner, M. Brandt, J. Cowell, T. Demuth, D. Vugts, G. Gasser, T.L. Mindt, The race for Hydroxamate-based Zirconium-89 chelators, Cancers 13 (2021) 4466, https://doi.org/10.3390/cancers13174466.
[6] W.E. Meijs, J.D.M. Herscheid, H.J. Haisma, H.M. Pinedo, Evaluation of Desferal as a bifunctional chelating agent for labeling antibodies with Zr-89, Int. J. Radiat. Appl. Instrument. 43 (1992) 1443–1447, https://doi.org/10.1016/0883-2889(92)90170-J.
[7] R.G. Pearson, Hard and soft acids and bases, J. Am. Chem. Soc. 85 (1963) 3533–3539, https://doi.org/10.1021/ja00905a001.
[8] D. Bellotti, M. Remelli, Deferoxamine B: a natural, excellent and versatile metal chelator, Molecules 26 (2021) 3255, https://doi.org/10.3390/molecules26113255.
[9] A. Werner, Zur Theorie Der Beizenfarbstoffe, Ber. Dtsch. Chem. Ges. 41 (1908) 1062–1071, https://doi.org/10.1002/cber.190804101210.
[10] F. Baroncelli, G. Grossi, The complexing power of Hydroxamic acids and its effect on the behaviour of organic Extractants in the reprocessing of irradiated fuels—I the complexes between Benzohydroxamic acid and zirconium, Iron (III) and uranium (VI), J. Inorg. Nucl. Chem. 27 (1965) 1085–1092, https://doi.org/10.1016/0022-1902(65)80420-1.
[11] G. Anderegg, F. L'Eplattenier, G. Schwarzenbach, Hydroxamatkomplexe II. Die Anwendung Der PH-Methode, Helvetica Chimica Acta 46 (1963) 1400–1408, https://doi.org/10.1002/hlca.19630460435.
[12] F. Guérard, Y.-S. Lee, R. Tripier, L.P. Szajek, J.R. Deschamps, M.W. Brechbiel, Investigation of Zr(IV) and 89Zr(IV) complexation with Hydroxamates: Progress towards designing a better Chelator than Desferrioxamine B for Immuno-PET imaging, Chem. Commun. 49 (2013) 1002–1004, https://doi.org/10.1039/C2CC37549D.
[13] A. Bianchi, M. Savastano, Comment on "Investigation of Zr(IV) and 89Zr(IV) Complexation with Hydroxamates: Progress towards Designing a Better Chelator than Desferrioxamine B for Immuno-PET Imaging" by F. Guérard, Y.-S. Lee, R. Tripier, L. P. Szajek, J. R. Deschamps and M. W. Brechbiel, Chem. Commun., 2013, 49, 1002, Chem. Commun. 56 (2020) 12664–12666, https://doi.org/10.1039/D0CC01189D.
[14] M. Savastano, C. Bazzicalupi, G. Ferraro, E. Fratini, P. Gratteri, A. Bianchi, Tales of the unexpected: the case of zirconium(IV) complexes with Desferrioxamine, Molecules 24 (2019) 2098, https://doi.org/10.3390/molecules24112098.
[15] Y. Toporivska, E. Gumienna-Kontecka, The solution thermodynamic stability of Desferrioxamine B (DFO) with Zr(IV), J. Inorg. Biochem. 198 (2019), 110753, https://doi.org/10.1016/j.jinorgbio.2019.110753.
[16] R. Imura, H. Ida, I. Sasaki, N.S. Ishioka, S. Watanabe, Re-evaluations of Zr-DFO complex coordination chemistry for the estimation of radiochemical yields and Chelator-to-antibody ratios of 89Zr immune-PET tracers, Molecules 26 (2021) 4977, https://doi.org/10.3390/molecules26164977.
[17] M. Savastano, F. Boscaro, A. Bianchi, Metal coordination properties of a Chromophoric Desferrioxamine (DFO) derivative: insight on the coordination stoichiometry and thermodynamic stability of Zr4+ complexes, Molecules 27 (2022) 184, https://doi.org/10.3390/molecules27010184.
[18] V. Liapis, W. Tieu, S.E. Rudd, P.S. Donnelly, N.L. Wittwer, M.P. Brown, A. H. Staudacher, Improved non-invasive positron emission tomographic imaging of chemotherapy-induced tumor cell death using Zirconium-89-labeled APOMAB®, EJNMMI Radiopharm. Chem. 5 (2020) 27, https://doi.org/10.1186/s41181-020-00109-6.
[19] I. Verel, G.W.M. Visser, R. Boellaard, M. Stigter-van Walsum, G.B. Snow, G.A.M. S. van Dongen, 89Zr Immuno-PET: comprehensive procedures for the production of 89Zr-labeled monoclonal antibodies, J. Nucl. Med. 44 (2003) 1271–1281.
[20] J.P. Holland, G. Normand, A. Ruggiero, J.S. Lewis, J. Grimm, Intraoperative imaging of positron emission tomographic radiotracers using Cerenkov luminescence emissions, Mol. Imaging 10 (2011), https://doi.org/10.2310/7290.2010.00047, 7290.2010.00047.
[21] A. Guillou, A. Ouadi, J.P. Holland, Heptadentate chelates for 89Zr-Radiolabelling of monoclonal antibodies, Inorg. Chem. Front. 9 (2022) 3071–3081, https://doi.org/10.1039/D2QI00442A.
[22] J.P. Holland, Predicting the thermodynamic stability of zirconium radiotracers, Inorg. Chem. 59 (2020) 2070–2082, https://doi.org/10.1021/acs.inorgchem.9b03515.
[23] S.D. Lytton, B. Mester, J. Libman, A. Shanzer, Z. Ioav Cabantchik, Monitoring of Iron(III) removal from biological sources using a fluorescent Siderophore, Anal. Biochem. 205 (1992) 326–333, https://doi.org/10.1016/0003-2697(92)90443-B.
[24] F. Delattre, F. Cazier-Dennin, L. Leleu, D. Dewaele, D. Landy, I. Mallard, P.-E. Danjou, Recognition of iron ions by carbazole–desferrioxamine fluorescent sensor and its application in total iron detection in airbone particulate matter, Talanta 144 (2015) 451–455, https://doi.org/10.1016/j.talanta.2015.06.071.
[25] M.E. Noltes, G.M. van Dam, W.B. Nagengast, P.J. van der Zaag, R.H.J.A. Slart, W. Szymanski, S. Kruijff, R.A.J.O. Dierckx, Let's embrace optical imaging: a growing branch on the clinical molecular imaging tree, Eur. J. Nucl. Med. Mol. Imaging 48 (2021) 4120–4128, https://doi.org/10.1007/s00259-021-05476-z.
[26] T.A. Pringle, C.D. Chan, S. Luli, H.J. Blair, K.S. Rankin, J.C. Knight, Synthesis and in vivo evaluation of a site-specifically labeled radioimmunoconjugate for dual-modal (PET/NIRF) imaging of MT1-MMP in sarcomas, Bioconjug. Chem. 33 (2022) 1564–1573, https://doi.org/10.1021/acs.bioconjchem.2c00306.
[27] J. Van Gompel, G.B. Schuster, Chemiluminescence of organic peroxides: intramolecular electron-exchange luminescence from a secondary perester, J. Organomet. Chem. 52 (1987) 1465–1468, https://doi.org/10.1021/jo00384a015.

[28] L. Allott, C.D. Pieve, J. Meyers, T. Spinks, D.M. Ciobota, G. Kramer-Marek, G. Smith, Evaluation of DFO-HOPO as an Octadentate Chelator for Zirconium-89, Chem. Commun. 53 (2017) 8529–8532, https://doi.org/10.1039/C7CC03572A.
[29] M. Fontanelli, M. Micheloni, In Proceedings of the Proceedings of the I Spanish-Italian Congress on Thermodynamics of Metal Complexes; Diputación de Castellón, Castellón (Spain), 1990, pp. 41–43.
[30] M. Savastano, M. Fiaschi, G. Ferraro, P. Gratteri, P. Mariani, A. Bianchi, C. Bazzicalupi, Sensing Zn2+ in aqueous solution with a fluorescent Scorpiand macrocyclic ligand decorated with an anthracene bearing tail, Molecules 25 (2020) 1355, https://doi.org/10.3390/molecules25061355.
[31] G. Gran, Determination of the equivalence point in potentiometric titrations. Part II, Analyst 77 (1952) 661–671, https://doi.org/10.1039/AN9527700661.
[32] P. Gans, A. Sabatini, A. Vacca, Investigation of equilibria in solution. Determination of equilibrium constants with the HYPERQUAD suite of programs, Talanta 43 (1996) 1739–1753, https://doi.org/10.1016/0039-9140(96)01958-3.
[33] M. Mangoni, M. Sottili, G. Salvatore, I. Meattini, I. Desideri, D. Greto, M. Loi, C. Becherini, P. Garlatti, C.D. Paoli, et al., Enhancement of soft tissue sarcoma cell Radiosensitivity by poly(ADP-ribose) Polymerase-1 inhibitors, Rare 190 (2018) 464–472, https://doi.org/10.1667/RR15035.1.
[34] U. Haberkorn, M. Knopp, W. Schlegel, G. Gademann, W. Semmler, A.H. Gamroth, G. Brix, Radiodiagnostics and radiotherapy, in: Current Cancer Research 1992; Steinkopff: Heidelberg, 1992, pp. 119–138 (ISBN 978-3-662-11384-4.).
[35] J. Qian, M. Xia, W. Liu, L. Li, J. Yang, Y. Mei, Q. Meng, Y. Xie, Glabridin Resensitizes P-glycoprotein-overexpressing multidrug-resistant Cancer cells to conventional chemotherapeutic agents, Eur. J. Pharmacol. 852 (2019) 231–243, https://doi.org/10.1016/j.ejphar.2019.04.002.
[36] Y.G. Assaraf, A. Brozovic, A.C. Gonçalves, D. Jurkovicova, A. Linē, M. Machuqueiro, S. Saponara, A.B. Sarmento-Ribeiro, C.P.R. Xavier, M. H. Vasconcelos, The multi-factorial nature of clinical multidrug resistance in Cancer, Drug Resist. Updat. 46 (2019), 100645, https://doi.org/10.1016/j.drup.2019.100645.
[37] J.W. Harper, S.J. Elledge, The DNA damage response: ten years after, Mol. Cell 28 (2007) 739–745, https://doi.org/10.1016/j.molcel.2007.11.015.
[38] D. Bani, A. Bencini, Developing ROS scavenging agents for pharmacological purposes: recent advances in design of manganese-based complexes with anti-inflammatory and anti- nociceptive activity, Curr. Med. Chem. 19 (2012) 4431–4444.
[39] H. Wang, X. Mu, H. He, X.-D. Zhang, Cancer Radiosensitizers, Trends Pharmacol. Sci. 39 (2018) 24–48, https://doi.org/10.1016/j.tips.2017.11.003.
[40] C.-Y. Ke, C.J. Mathias, M.A. Green, Folate-receptor-targeted radionuclide imaging agents, Adv. Drug Deliv. Rev. 56 (2004) 1143–1160, https://doi.org/10.1016/j.addr.2004.01.004.
[41] F. Kraeber-Bodéré, C. Rousseau, C. Bodet-Milin, C. Mathieu, F. Guérard, E. Frampas, T. Carlier, N. Chouin, F. Haddad, J.-F. Chatal, et al., Tumor Immunotargeting using innovative radionuclides, Int. J. Mol. Sci. 16 (2015) 3932–3954, https://doi.org/10.3390/ijms16023932. Graphical Abstract.